NANO LETTERS

pubs.acs.org/NanoLett Letter

Electrically Reconfigurable Plasmonic Metasurfaces Based on Phase-Change Materials Sb_2S_3

Zhuoxuan Han, Chensheng Li, Tengzhang Liu, Nannan Hu, Zhiqin Fan, Yang Guo, Baoli Liu, Haifang Yang, Aizi Jin, Baogang Quan, Shibing Tian, Yang Yang, Geng Li, Xiaofeng Fan, Sha Hu,* Xin Huang,* and Changzhi Gu*

Cite This: *Nano Lett.* 2025, 25, 7435−7441 Read Online

ACCESS | Metrics & More | Article Recommendations | Supporting Information

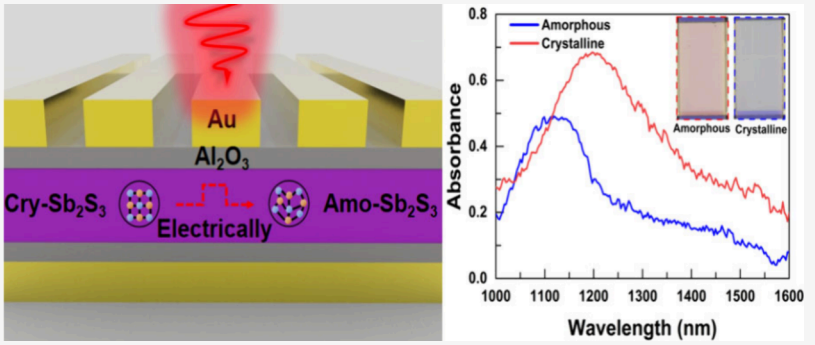

ABSTRACT: Phase-change materials (PCMs) are widely used in active optical metasurfaces due to their large refractive index contrast and fast and stable phase-change properties. In this paper, an electrically reconfigurable plasmonic metasurface based on the PCM Sb_2S_3 is proposed to achieve nonvolatile, reversible, and fast optical modulation in the near-infrared range. The designed metasurface can redshift the surface plasmon resonance peak from 1320 to 1480 nm through the phase transition of Sb_2S_3 from amorphous to crystalline states. In addition, we further experimentally design an electrically reconfigurable platform. In a 30 μm × 30 μm region, the phase state of Sb_2S_3 with a thickness of 60 nm is successfully and reversibly changed, which contributes to the dynamic modulation of gold gratings. This work has great application potential in reconfigurable optical filters and communication systems and adaptive optical imaging and sensing.

KEYWORDS: *metasurface, electrical tuning, reversible switching, phase-change material*

Metamaterials are artificial materials whose dimensions are smaller than the wavelength of external excitation. Unlike natural materials, whose electromagnetic properties are determined by the specific characteristics of their atoms or molecules, metamaterials can be artificially tailored to engineer desired electromagnetic responses.[1] Therefore, metamaterials can flexibly manipulate the properties of electromagnetic waves such as amplitude, polarization, and phase. Subsequently, extraordinary characteristics not found in natural materials can be achieved by metasurfaces, such as abnormal deflection,[2,3] metalenses,[4,5] and perfect absorption.[6,7] As a two-dimensional metamaterial, metasurfaces can not only flexibly manipulate electromagnetic wave characteristics[8,9] but also have the advantages of flexible design, small size, and easy integration compared with metamaterials.

Once most metasurfaces are fabricated, their functions will be fixed and lack dynamic tuning, which limits their breakthrough in practical applications. Active metasurfaces can dynamically modulate their optical responses, providing exciting opportunities for flexible manipulation of light propagation.[10,11] So far, the active tuning of metasurfaces has been utilized through mechanical deformation,[12−14] electrochemical or chemical reaction,[15] electrical regulation,[16−18] and all-optical regulation.[19] In addition, liquid-crystal materials[20] and phase-change materials (PCMs)[21−24] are often used in active metasurfaces. In particular, PCMs have unique conditions for achieving active modulation due to the significant refractive index contrast brought about by their structural transitions. PCMs have been widely applied in reconfigurable photonic platforms, extending from programmable photonics, neuromorphic computing, and nonvolatile and rewritable data storage to tunable metasurfaces. For PCM-

Received: February 11, 2025
Revised: April 21, 2025
Accepted: April 21, 2025
Published: April 23, 2025

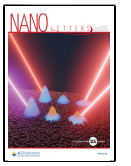

https://doi.org/10.1021/acs.nanolett.5c00929
Nano Lett. 2025, 25, 7435−7441

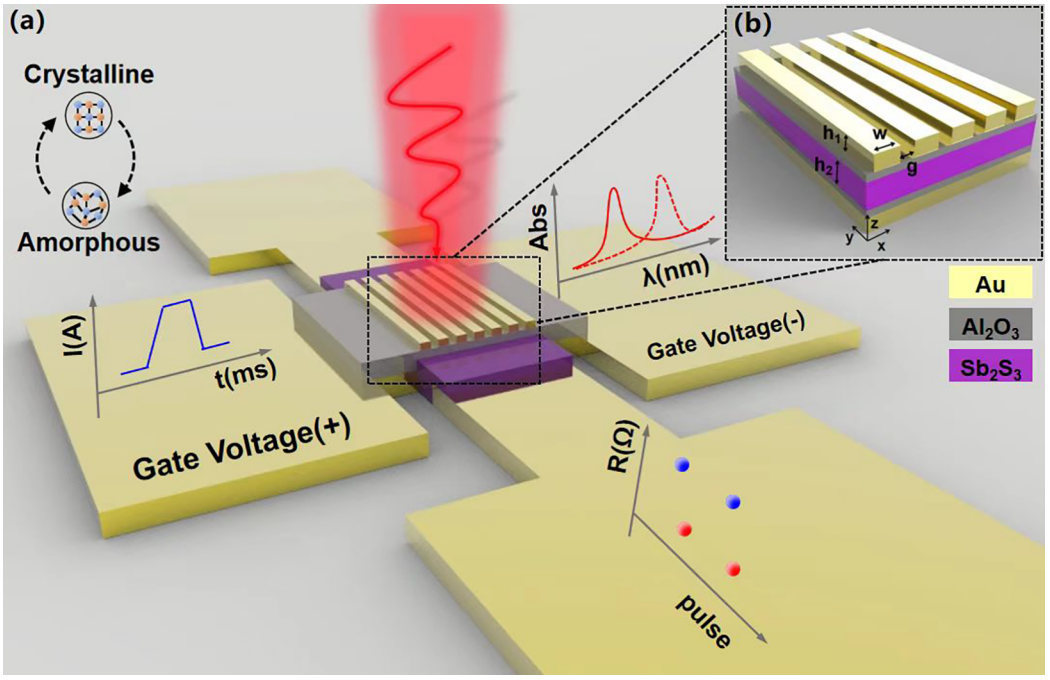

Figure 1. Operation and optical response of an electrically tunable Sb_2S_3-based metasurface. (a) Schematic diagram of the electrothermal metasurface. The tunable metasurface makes the Sb_2S_3 phase change by applying a voltage and shows a dynamic modulation of the plasmon resonance in the near-infrared band. The corresponding geometric parameters are shown in part b.

based metasurfaces, dynamic switching can be realized between amorphous and crystalline states by thermal annealing or laser pulse excitation. Additionally, the electrical switching of PCMs naturally favors compact integration with planar optics and anticipates miniaturization, leading to chip-level reconfigurable optical systems.

$Ge_2Sb_2Te_5$ (GST), one of the most common PCMs, has a large refractive index contrast in the near-infrared band. GST-based metasurfaces have a wide range of applications in holographic imaging,[25,26] perfect absorption,[27] and other fields. However, the crystalline GST has a large loss, which also limits its performance in the field of photoelectric detection. Antimony sulfide (Sb_2S_3) has recently been classified as a PCM.[28−30] Compared with GST, Sb_2S_3 has almost zero loss in the near-infrared band. This type of material can be stimulated between its amorphous and crystalline phases through thermal or laser irradiation, requiring modulation of its refractive index in an ultrashort time (on the order of picoseconds).[31,32] However, both methods require bulky external equipment, namely, heating stages or ultrafast lasers. Therefore, electric drive regulation becomes the best choice for the active regulation of PCM metasurfaces. Compared with the electric regulation of other materials,[33,34] PCMs have the advantages of fast response speed. Currently, there have been reports of electrical-driven control based on GST.[35,36] However, the electrical control of Sb_2S_3 still poses challenges because the crystallization temperature of Sb_2S_3 is around 270 °C, which is much higher than that of GST. Additionally, high temperatures can cause thermal deformation of the surrounding nanostructures. Nevertheless, recent advancements have achieved electrothermal control of Sb_2S_3 using microheaters.

In this work, we propose a metal−insulator−metal (MIM) structure that consists of a gold (Au) substrate, PCM Sb_2S_3, and a gold grating. For the proposed metasurface, the plasmon resonance of the surface grating is dynamically adjusted by the huge refractive index difference generated by the Sb_2S_3 phase transition. Furthermore, we demonstrate on-demand optical modulation and wavefront engineering in a 30 μm × 30 μm area using electrical drive, achieving a fully reversible and reconfigurable Sb_2S_3-based metasurface. The design proposed in this paper can produce a spectral response that is more sensitive to incident polarization with potential applications in imaging, information transmission, and photoelectric detection.

An electrically tunable metasurface based on Sb_2S_3 is demonstrated, as schematically shown in Figure 1a. The metasurface is composed of gold gratings and a microheater, which are separated by Al_2O_3 and Sb_2S_3 films. The gold grating controls the excitation and characteristics of the surface plasmon through varying specific structural parameters and environmental conditions. The microheater is composed of 5 nm of titanium and 60 nm of gold. The electrodes at the left and right ends are responsible for applying the voltage required for the phase transition of Sb_2S_3. The electrodes at the upper and lower ends are directly connected to Sb_2S_3 to measure the resistance of Sb_2S_3. The entire microheater is mounted on a silica substrate, which effectively prevents heat loss. Under the conditions of external voltage pulse excitation, the Sb_2S_3 film can be transformed between the amorphous phase and the crystalline phase. In addition, because Sb_2S_3 is nonvolatile, crystalline and amorphous states can be activated and maintained. The phase transition of Sb_2S_3 results in a great change of its dielectric constant changes, leading to a red shift of the resonance wavelength. The corresponding structural parameters of our proposed tunable metasurface are marked in Figure 1b, where h_1 and h_2 represent the height of the gold grating and Sb_2S_3, respectively, w is the width of the gold grating, and g is the spacing between the gratings.

The finite-difference time-domain (FDTD) method is used to numerically optimize the structure design. In this study, the

https://doi.org/10.1021/acs.nanolett.5c00929
Nano Lett. 2025, 25, 7435−7441

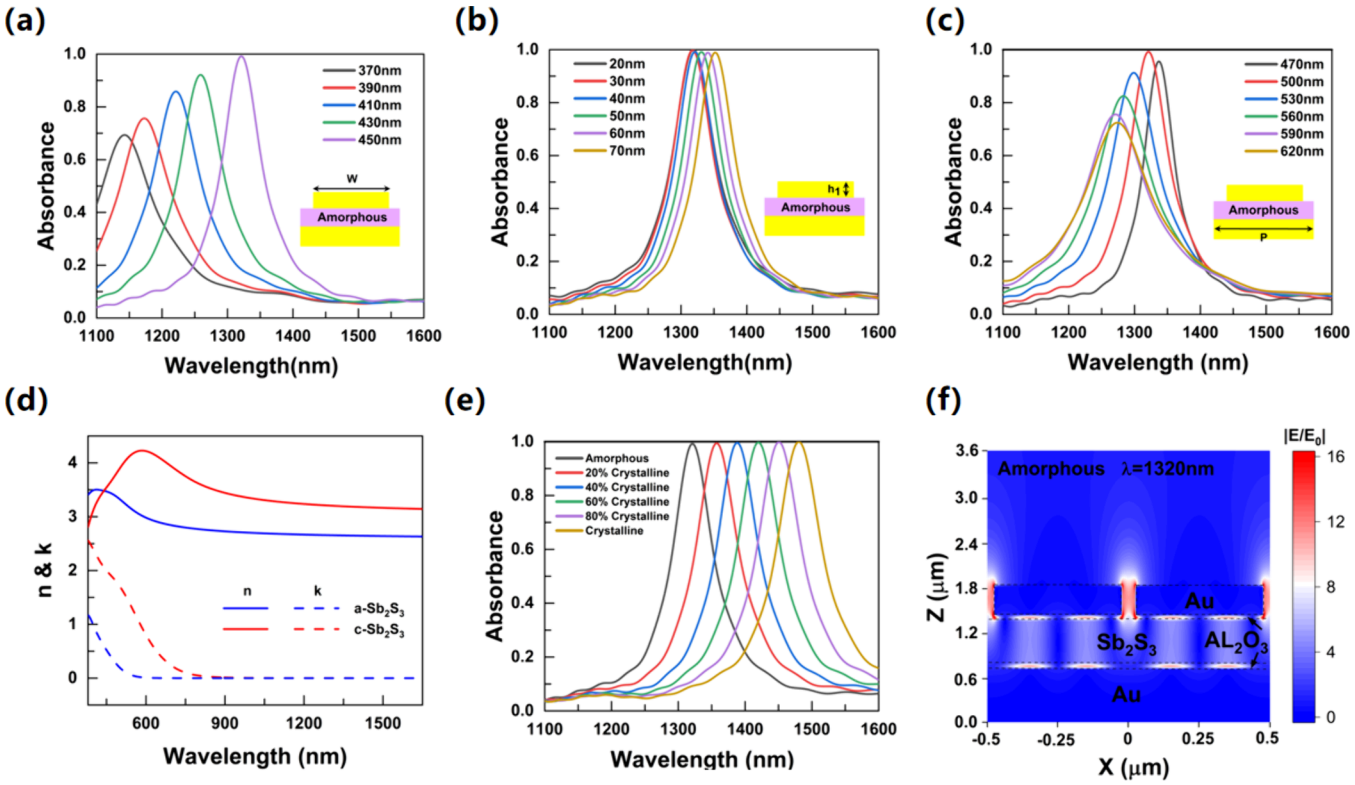

Figure 2. Simulated results of demonstrated metasurfaces under different structural parameters. Simulated absorption spectra when the gold gratings have varied (a) widths, (b) periods, and (c) thicknesses. (d) Measured complex refractive indices for amorphous and crystallized films of Sb_2S_3. (e) Simulated absorbance spectra of the active phase-change metasurface with different crystallization fractions of Sb_2S_3. (f) Electric-field distribution of the metasurfaces in the a-Sb_2S_3 case at a wavelength of 1320 nm.

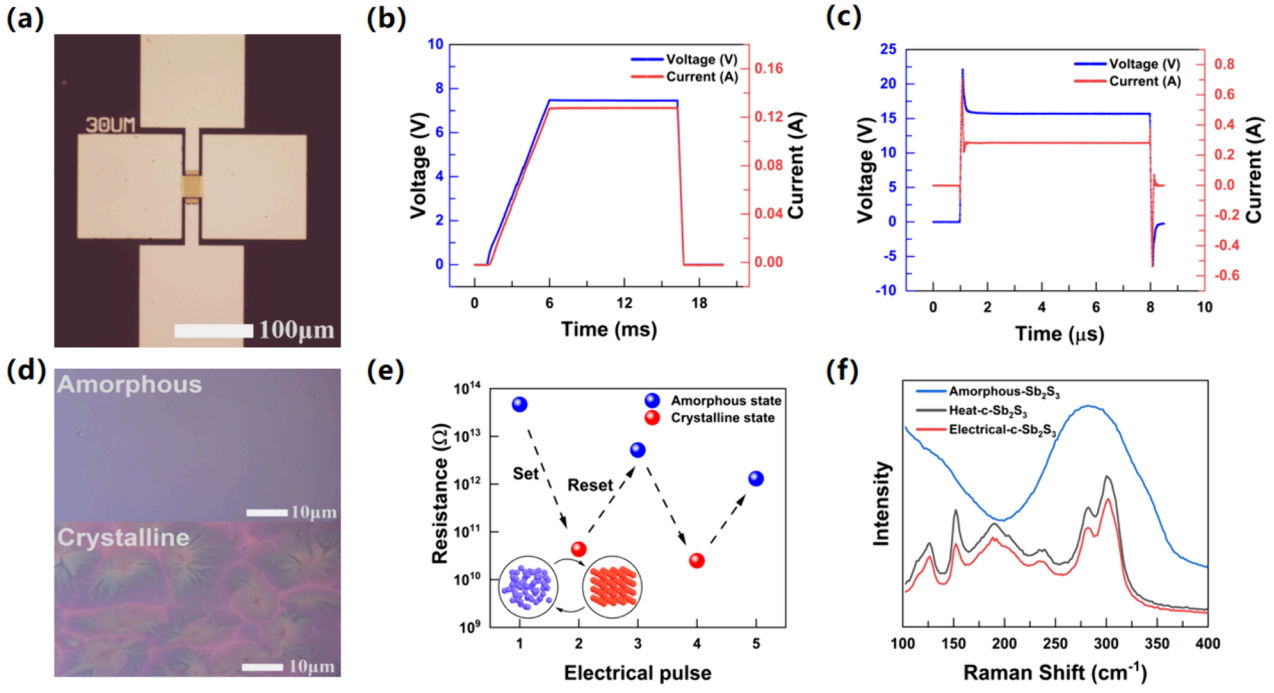

Figure 3. Electrically driven phase change of the Sb_2S_3 layer based on a microheater. (a) Optical micrograph of the sample. The applied current and voltage of the (b) "set" and (c) "reset" pulses varying with time. (d) Optical micrograph of amorphous (up) and crystalline (down) Sb_2S_3. (e) Measured resistance of the Sb_2S_3 film after each pulse, where blue dots represent the resistance with "reset" pulse and red dots denote the resistance with "set" pulse. The robust and reversible switching between the crystalline and amorphous phases is confirmed by resistance changes exceeding 1 order of magnitude. (f) Raman spectra of amorphous Sb_2S_3, high-temperature-annealed crystalline Sb_2S_3, and electrically controlled crystalline Sb_2S_3.

https://doi.org/10.1021/acs.nanolett.5c00929
Nano Lett. 2025, 25, 7435−7441

1300−1500 nm communication band, which is the most common working wavelength in integrated photonics, is chosen. Moreover, the incident light is polarized along the x direction. Parts a−c of Figure 2 display the simulated absorption spectra when the metasurface has varied structural parameters and is in the amorphous state of Sb_2S_3. The period was first fixed to 500 nm, with h_1 = 40 nm and h_2 = 60 nm, and the widths of the gold gratings varied from 370 to 450 nm. As shown in Figure 2a, when the width increases, the absorption peak becomes narrower and stronger, resulting in a higher absorbance. The absorbance reaches nearly one unit at w = 450 nm, so the width is fixed at 450 nm. Under the same geometric conditions, the absorption spectra of crystalline Sb_2S_3 with geometric parameter w are also discussed in Figure S1. It indicates that the results are consistent with those of the amorphous state, as shown. The influence of the thickness of the top gold nanoantenna in Figure 2b was also discussed (w = 450 nm and g = 50 nm). The corresponding full width at half-maximum and absorbance are detailed in Figure S1. The simulated spectra indicate that 40 nm is the optimal thickness. Figure 2c shows the absorption spectra under different periods. When the width of the gold grating is fixed at 450 nm, h_1 = 40 nm, it can be clearly seen that the absorption spectra have an increasing trend by reducing the period. When the period is 500 nm, the absorbance reaches almost 1. When the period continues to decrease, the absorption spectra show a downward trend. Therefore, the period is fixed at 500 nm. Through structural optimization, the parameters of the metasurface were finally determined to be h_1 = 40 nm, h_2 = 60 nm, w = 450 nm, and g = 50 nm.

Subsequently, the effect of the phase state of Sb_2S_3 on the absorption resonance of the designed metasurface is analyzed. The measured refractive index and extinction coefficient of Sb_2S_3 are displayed in Figure 2d, which show a strong refractive index contrast in the near-infrared band. The resonance peak can be regulated due to the refractive index contrast between crystalline Sb_2S_3 (c-Sb_2S_3) and amorphous Sb_2S_3 (a-Sb_2S_3). Furthermore, the effective modulation of the resonance wavelength can be achieved when Sb_2S_3 is in different degrees of crystallization. As shown in Figure 2e, the resonance peak moves from 1320 to 1480 nm before and after the phase transition of Sb_2S_3 and undergoes a shift of about 160 nm. The whole structure is in the communication band, which is of great significance for high-performance near-infrared photoelectric detection. Figure 2f shows the electric-field distribution of the designed metasurface with amorphous Sb_2S_3 at 1320 nm. It indicates that the electric field is mainly concentrated on the two edges of the metal nanoantenna, which satisfies the typical characteristics of plasma resonance. Our structural configuration significantly enhances the interaction between light and the Sb_2S_3 layer. When the Sb_2S_3 layer is in different crystalline components, the effective refractive index of the surface plasmon gap changes significantly, thereby expanding the wavelength range of spectral tuning.

For our proposed tunable metasurface, an electrothermal approach is employed to achieve dynamic and reversible phase change of the Sb_2S_3 layer. The electrically driven phase change is based on a microheater, whose optical microscopy image is shown in Figure 3a. Different sizes of square Sb_2S_3-based metasurfaces were prepared. However, with expansion of the aperture size of the metasurface, the mitigation of thermal inhomogeneity becomes a key challenge. Therefore, the size of the heating area is 30 μm × 30 μm, and the area of Sb_2S_3 is 20 μm × 30 μm. It can be seen from Figure 3a that the electrodes at both ends are directly connected to the microheating plate. Among them, the microheating plate is responsible for applying an electric pulse to actively regulate the phase state of Sb_2S_3 in the central heating area. The upper and lower electrodes are directly connected to Sb_2S_3, which is responsible for measuring the resistance of Sb_2S_3 to determine whether it is a phase transition. The manufacturing process is described in detail in Figure S3.

In each device, the phase state of Sb_2S_3 is jointly controlled by electrical pulses, i.e., "set" and "reset". Long and low voltage pulses (16 ms, <7.5 V) trigger crystallization by Joule heating, as shown in Figure 3b. The short and high voltage pulse (8 μs, 15.7 V) reamorphizes the elemental atoms (∼550 °C) through the melt-quenching process, as displayed in Figure 3c. It is worth noting that the high-voltage pulse has extremely short front and rear edges (∼0.05 μs). This allows Sb_2S_3 to be rapidly heated and melted and then rapidly cooled to solidify amorphously. Compared with the previously reported GST regulation,[35,36] our regulation time is a little longer. The time factor is attributed to the size of the heater region, the material, and the thickness of the PCM. Furthermore, under identical conditions, Sb_2S_3 exhibits slower switching speeds than GST due to its significantly higher phase transition temperature (∼270 vs ∼160 °C for GST).

The amorphization process requires a sufficiently fast cooling rate. Due to the poor thermal conductivity of silicon oxide, this is also an important factor in the selection of silicon oxide for our substrate. In addition, when the phase of Sb_2S_3 is switched, a rapid color change occurs due to the change of its optical constant, as shown in Figure 3d. Optical micrographs of amorphous and crystalline Sb_2S_3 films are shown (the up side is the amorphous state, and the down side represents the crystalline state). The surface of crystalline Sb_2S_3 shows obvious crystalline silk, and the change of the surface morphology indicates that the phase transition of Sb_2S_3 can be regulated by an electric pulse.

The upper and lower electrodes monitor the resistance of the Sb_2S_3 film after an electrical pulse. The switching behavior of Sb_2S_3 was further analyzed, as shown in Figure 3e. The resistance after each set pulse continuously reduced by at least 2 orders of magnitude, while the resistance after each reset pulse is opposite. It is confirmed that reversible switching between the a-Sb_2S_3 and c-Sb_2S_3 stages can be achieved. The slight change in resistance during the reset process may indicate that c-Sb_2S_3 is not completely reamorphous, as shown in Figure S4.

Figure 3f shows Raman spectra evidencing the transition from amorphous to crystalline Sb_2S_3 states. The blue line is the Raman spectrum of the amorphous Sb_2S_3 film, which has two broad bands at ∼290 and ∼100 cm^{-1}. These bands correspond to the vibrational Sb−Sb bonds in the $S_2Sb-SbS_2$ structural unit and the Sb_2S_3 pyramid, respectively.[37,38] Black and red lines represent the Raman spectra of crystalline Sb_2S_3 annealed at 300 °C on a hot plate and electrically tuned by a microheater, respectively. The band at 290 cm^{-1} is split into two sub-bands, and the band at ∼100 cm^{-1} is further split into many small peaks. These characteristics are consistent with the Raman spectra of the reported crystalline-state Sb_2S_3 film.[39] Therefore, the feasibility of electrically tuning Sb_2S_3 is also confirmed.

https://doi.org/10.1021/acs.nanolett.5c00929
Nano Lett. 2025, 25, 7435−7441

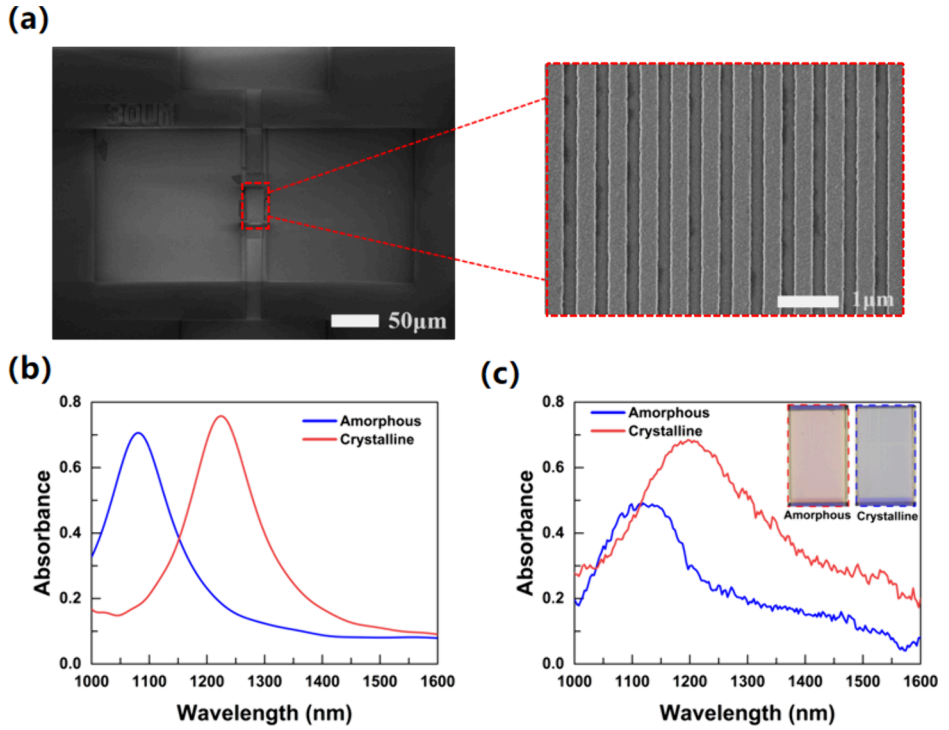

Figure 4. Electorally reconfigurable plasmon metasurface. (a) SEM images of actively regulated plasmonic metasurfaces. (b) Simulated absorption spectra of the a-Sb_2S_3 and c-Sb_2S_3 metasurfaces with a period of 500 nm and a gold grating width of 340 nm. (c) Measured absorption of the metasurface after a set pulse.

Due to the limitation of experimental conditions, a grating structure with p = 500 nm and w = 340 nm was fabricated. Figure 4a shows a scanning electron microscopy (SEM) image of the combination of a gold grating and a microheater. The simulated absorption spectra of the Sb_2S_3-based metasurface before and after the phase transition are shown in Figure 4b. The resonance peak shifts to 140 nm after the phase transition. The corresponding measured absorption spectra are displayed in Figure 4c. The peak position and intensity of the experimental spectra are basically consistent with those of the simulated results. The peak is 1109 nm in the amorphous state. After the reset pulse, the resonance peak red-shifts to 1206 nm, and the resonance peak moves 97 nm before and after the phase transition. Because the melting point of gold nanorods is much lower than that of bulk gold, the displacement difference is partly caused by thermal melting of the top gold grating,[40−42] as shown in Figure S5. In addition, Figure 4c also shows the optical micrographs of the Sb_2S_3 metasurface before and after the phase transition. It can be seen that the color of the metasurface changes significantly after the reset pulse is applied, which is also caused by the Sb_2S_3 phase transition.

In summary, we have experimentally demonstrated an electrically reconfigurable Sb_2S_3-based metasurface. The metasurface adopts an MIM-type structure, and multistage continuous operation of infrared resonance absorption can be achieved by changing the crystal state of Sb_2S_3. In addition, compared with vanadium oxide, Sb_2S_3 is not volatile and can activate and maintain crystalline and amorphous states. Compared with GST, the near-infrared extinction coefficient of Sb_2S_3 is almost zero. In the experiment, an electric microheater was designed to quasi-continuously, reversibly, and nonvolatilely drive the phase change of Sb_2S_3. The wavelength shift in the near-infrared spectral range has been experimentally demonstrated to be achieved by using an electric Sb_2S_3 metasurface. The measured red shift of the wavelength is 97 nm. Our findings can open up new directions for reconfigurable optical devices that can manipulate the main properties of light for various applications, including imaging, computing, and near-infrared photodetectors.

■ ASSOCIATED CONTENT

Supporting Information

The Supporting Information is available free of charge at https://pubs.acs.org/doi/10.1021/acs.nanolett.5c00929.

Simulation part, experimental preparation, sample characterization, optimization of the PCM metasurface, characterization of electrically tunable Sb_2S_3 surface morphology, experimental results of the Sb_2S_3-based metasurface, and the reflection spectrum under y polarization (PDF)

■ AUTHOR INFORMATION

Corresponding Authors

Sha Hu − *School of Physics, Henan University of Technology, Zhengzhou, Henan 450001, China;* orcid.org/0000-0002-3851-8003; Email: husha@haut.edu.cn

Xin Huang − *Beijing National Laboratory for Condensed Matter Physics, Institute of Physics, Chinese Academy of Sciences, Beijing 100190, China; School of Physical Sciences, CAS Key Laboratory of Vacuum Physics, University of Chinese Academy of Sciences, Beijing 100190, China;* Email: xinhuang@iphy.ac.cn

Changzhi Gu − *Beijing National Laboratory for Condensed Matter Physics, Institute of Physics, Chinese Academy of Sciences, Beijing 100190, China; School of Physical Sciences, CAS Key Laboratory of Vacuum Physics, University of*

https://doi.org/10.1021/acs.nanolett.5c00929
Nano Lett. 2025, 25, 7435−7441

Chinese Academy of Sciences, Beijing 100190, China; orcid.org/0000-0002-2689-2807; Email: czgu@iphy.ac.cn

Authors

Zhuoxuan Han − *Beijing National Laboratory for Condensed Matter Physics, Institute of Physics, Chinese Academy of Sciences, Beijing 100190, China; School of Physics, Henan University of Technology, Zhengzhou, Henan 450001, China;* orcid.org/0009-0007-1462-5799

Chensheng Li − *Beijing National Laboratory for Condensed Matter Physics, Institute of Physics, Chinese Academy of Sciences, Beijing 100190, China;* orcid.org/0000-0002-8902-6594

Tengzhang Liu − *Beijing National Laboratory for Condensed Matter Physics, Institute of Physics, Chinese Academy of Sciences, Beijing 100190, China*

Nannan Hu − *Beijing National Laboratory for Condensed Matter Physics, Institute of Physics, Chinese Academy of Sciences, Beijing 100190, China; School of Physics, Henan University of Technology, Zhengzhou, Henan 450001, China*

Zhiqin Fan − *School of Physics, Henan University of Technology, Zhengzhou, Henan 450001, China*

Yang Guo − *Beijing National Laboratory for Condensed Matter Physics, Institute of Physics, Chinese Academy of Sciences, Beijing 100190, China; School of Physical Sciences, CAS Key Laboratory of Vacuum Physics, University of Chinese Academy of Sciences, Beijing 100190, China;* orcid.org/0000-0001-8975-9387

Baoli Liu − *Beijing National Laboratory for Condensed Matter Physics, Institute of Physics, Chinese Academy of Sciences, Beijing 100190, China; School of Physical Sciences, CAS Key Laboratory of Vacuum Physics, University of Chinese Academy of Sciences, Beijing 100190, China*

Haifang Yang − *Beijing National Laboratory for Condensed Matter Physics, Institute of Physics, Chinese Academy of Sciences, Beijing 100190, China*

Aizi Jin − *Beijing National Laboratory for Condensed Matter Physics, Institute of Physics, Chinese Academy of Sciences, Beijing 100190, China*

Baogang Quan − *Beijing National Laboratory for Condensed Matter Physics, Institute of Physics, Chinese Academy of Sciences, Beijing 100190, China*

Shibing Tian − *Beijing National Laboratory for Condensed Matter Physics, Institute of Physics, Chinese Academy of Sciences, Beijing 100190, China*

Yang Yang − *Beijing National Laboratory for Condensed Matter Physics, Institute of Physics, Chinese Academy of Sciences, Beijing 100190, China;* orcid.org/0000-0003-3785-9233

Geng Li − *School of Physical Sciences, CAS Key Laboratory of Vacuum Physics, University of Chinese Academy of Sciences, Beijing 100190, China;* orcid.org/0000-0002-3347-7222

Xiaofeng Fan − *Key Laboratory of Automobile Materials (Jilin University), Ministry of Education, and College of Materials Science and Engineering, Jilin University, Changchun 130012, China;* orcid.org/0000-0001-6288-4866

Complete contact information is available at: https://pubs.acs.org/10.1021/acs.nanolett.5c00929

Author Contributions

Z.H. and X.H. conceived the initial idea of electrically reconfigurable plasmonic metasurfaces based on the PCM Sb_2S_3. Z.H. and X.H. developed the theory and performed numerical simulations with the help of T.L., N.H., and Z.F.. Z.H. and S.H. prepared the manuscript. Z.H. conducted the experiment and performed the tests with the help of C.L., Y.G., B.L., H.Y., A.J., B.Q., S.T., Y.Y., G.L., and X.F.. Z.H., S.H., and C.G. supervised the overall project. All of the authors analyzed the data and discussed the results.

Notes

The authors declare no competing financial interest.

■ ACKNOWLEDGMENTS

This work was supported by the National Key Research and Development Program of China (Grants 2024YFA1207700, 2022YFA1204100, and 2021YFA1400700), the National Natural Science Foundation of China (Grants 12104133, 92265110, 62174179, and 62204259), the Strategic Priority Research Program of Chinese Academy of Sciences (CAS) (Grant XDB33020200), the Talent Introduction Fund at Henan University of Technology (Grant 2020BS057), and the Open Research Fund of Beijing National Laboratory for Condensed Matter Physics (2024BNLCMPKF014). This work was also supported by the Micro/nano Fabrication Laboratory of Synergetic Extreme Condition User Facility.

■ REFERENCES

(1) Zheludev, N. I. The Road Ahead for Metamaterials. *Science* **2010**, *328* (5978), 582−583.

(2) He, T.; Liu, T.; Xiao, S. Y.; Wei, Z. Y.; Wang, Z. S.; Zhou, L.; Cheng, X. B. Perfect anomalous reflectors at optical frequencies. *Sci. Adv.* **2022**, *8* (9), 9.

(3) Abdollahramezani, S.; Hemmatyar, O.; Taghinejad, M.; Taghinejad, H.; Kiarashinejad, Y.; Zandehshahvar, M.; Fan, T. R.; Deshmukh, S.; Eftekhar, A. A.; Cai, W. S.; et al. Dynamic Hybrid Metasurfaces. *Nano Lett.* **2021**, *21* (3), 1238−1245.

(4) Li, S. Y.; Zhou, C. B.; Ban, G. X.; Wang, H.; Lu, H.; Wang, Y. Active all-dielectric bifocal metalens assisted by germanium antimony telluride. *J. Phys. D: Appl. Phys.* **2019**, *52* (9), 095106.

(5) Zheng, R.; Pan, R.; Geng, G.; Jiang, Q.; Du, S.; Huang, L.; Gu, C.; Li, J. Active multiband varifocal metalenses based on orbital angular momentum division multiplexing. *Nat. Commun.* **2022**, *13* (1), 4292.

(6) Hu, S.; Yang, S. Y.; Liu, Z.; Quan, B. G.; Li, J. J.; Gu, C. Z. Broadband and Polarization-Insensitive Absorption Based on a Set of Multisized Fabry-Perot-like Resonators. *J. Phys. Chem. C* **2019**, *123* (22), 13856−13862.

(7) Li, Y.; Lin, J.; Guo, H. J.; Sun, W. J.; Xiao, S. Y.; Zhou, L. A Tunable Metasurface with Switchable Functionalities: From Perfect Transparency to Perfect Absorption. *Adv. Opt. Mater.* **2020**, *8* (6), 8.

(8) Lv, W. J.; Qin, H. Y.; Su, Z. P.; Zhang, C. Z.; Huang, J. P.; Shi, Y. Z.; Li, B.; Genevet, P.; Song, Q. H. Robust generation of intrinsic C points with magneto-optical bound states in the continuum. *Sci. Adv.* **2024**, *10* (46), 6.

(9) Qin, H. Y.; Su, Z. P.; Zhang, Z.; Lv, W. J.; Yang, Z. J.; Chen, W. J.; Gao, X. Y.; Wei, H.; Shi, Y. Z.; Li, B.; Zhou, J.; Fleury, R.; Qiu, C. W.; Song, Q. H. Disorder-assisted real-momentum topological photonic crystal. *Nature* **2025**, *639* (8055), 602−608.

(10) Shalaginov, M. Y.; Campbell, S. D.; An, S. S.; Zhang, Y. F.; Ríos, C.; Whiting, E. B.; Wu, Y. H.; Kang, L.; Zheng, B. W.; Fowler, C.; et al. Design for quality: reconfigurable flat optics based on active metasurfaces. *Nanophotonics* **2020**, *9* (11), 3505−3534.

(11) Kang, L.; Jenkins, R. P.; Werner, D. H. Recent Progress in Active Optical Metasurfaces. *Adv. Opt. Mater.* **2019**, *7* (14), 26.

(12) Ee, H. S.; Agarwal, R. Tunable Metasurface and Flat Optical Zoom Lens on a Stretchable Substrate. *Nano Lett.* **2016**, *16* (4), 2818−2823.

(13) Arbabi, E.; Arbabi, A.; Kamali, S. M.; Horie, Y.; Faraji-Dana, M.; Faraon, A. MEMS-tunable dielectric metasurface lens. *Nat. Commun.* **2018**, *9*, 9.
(14) She, A.; Zhang, S. Y.; Shian, S.; Clarke, D. R.; Capasso, F. Adaptive metalenses with simultaneous electrical control of focal length, astigmatism, and shift. *Sci. Adv.* **2018**, *4* (2), 7.
(15) Zanotto, S.; Blancato, A.; Buchheit, A.; Muñoz-Castro, M.; Wiemhöfer, H. D.; Morichetti, F.; Melloni, A. Metasurface Reconfiguration through Lithium-Ion Intercalation in a Transition Metal Oxide. *Adv. Opt. Mater.* **2017**, *5* (2), 6.
(16) Zhang, Y. F.; Fowler, C.; Liang, J. H.; Azhar, B.; Shalaginov, M. Y.; Deckoff-Jones, S.; An, S. S.; Chou, J. F. B.; Roberts, C. M.; Liberman, V.; et al. Electrically reconfigurable non-volatile metasurface using low-loss optical phase-change material. *Nat. Nanotechnol.* **2021**, *16* (6), 661−666.
(17) Liu, L.; Kang, L.; Mayer, T. S.; Werner, D. H. Hybrid metamaterials for electrically triggered multifunctional control. *Nat. Commun.* **2016**, *7*, 8.
(18) Zhou, W.; Farmakidis, N.; Feldmann, J.; Li, X.; Tan, J.; He, Y. H.; Wright, C. D.; Pernice, W. H. P.; Bhaskaran, H. Phase-change materials for energy-efficient photonic memory and computing. *MRS Bull.* **2022**, *47* (5), 502−510.
(19) Shcherbakov, M. R.; Vabishchevich, P. P.; Shorokhov, A. S.; Chong, K. E.; Choi, D. Y.; Staude, I.; Miroshnichenko, A. E.; Neshev, D. N.; Fedyanin, A. A.; Kivshar, Y. S. Ultrafast All-Optical Switching with Magnetic Resonances in Nonlinear Dielectric Nanostructures. *Nano Lett.* **2015**, *15* (10), 6985−6990.
(20) Komar, A.; Paniagua-Domínguez, R.; Miroshnichenko, A.; Yu, Y. F.; Kivshar, Y. S.; Kuznetsov, A. I.; Neshev, D. Dynamic Beam Switching by Liquid Crystal Tunable Dielectric Metasurfaces. *ACS Photonics* **2018**, *5* (5), 1742−1748.
(21) Pitchappa, P.; Kumar, A.; Prakash, S.; Jani, H.; Venkatesan, T.; Singh, R. Chalcogenide Phase Change Material for Active Terahertz Photonics. *Adv. Mater.* **2019**, *31* (12), 7.
(22) Abdollahramezani, S.; Hemmatyar, O.; Taghinejad, H.; Krasnok, A.; Kiarashinejad, Y.; Zandehshahvar, M.; Alù, A.; Adibi, A. Tunable nanophotonics enabled by chalcogenide phase-change materials. *Nanophotonics* **2020**, *9* (5), 1189−1241.
(23) Tian, J. Y.; Luo, H.; Yang, Y. Q.; Ding, F.; Qu, Y. R.; Zhao, D.; Qiu, M.; Bozhevolnyi, S. I. Active control of anapole states by structuring the phase-change alloy $Ge_2Sb_2T_5$. *Nat. Commun.* **2019**, *10*, 9.
(24) Leitis, A.; Hessler, A.; Wahl, S.; Wuttig, M.; Taubner, T.; Tittl, A.; Altug, H. All-Dielectric Programmable Huygens' Metasurfaces. *Adv. Funct. Mater.* **2020**, *30* (19), 8.
(25) Li, C.; Du, S.; Pan, R.; Xiong, X.; Tang, Z.; Zheng, R.; Liu, Y.; Geng, G.; Sun, J.; Gu, C.; Guo, H.; Li, J. Phase Change Materials-Based Bilayer Metasurfaces for Near-Infrared Photonic Routing. *Adv. Funct. Mater.* **2024**, *34* (14), 11.
(26) Hu, S.; Han, Z.; Du, S.; Wang, C.; Hu, N.; Fan, Z.; Huang, X.; Gu, C. Nonvolatile Switchable Janus Metasurface for Multi-Dimension Encoded Near- and Far-Field Functionalization. *Adv. Funct. Mater.* **2024**, 2419741.
(27) Qu, Y. R.; Li, Q.; Cai, L.; Pan, M. Y.; Ghosh, P.; Du, K. K.; Qiu, M. Thermal camouflage based on the phase-changing material GST. *Light Sci. Appl.* **2018**, *7*, 10.
(28) Dong, W. L.; Liu, H. L.; Behera, J. K.; Lu, L.; Ng, R. J. H.; Sreekanth, K. V.; Zhou, X. L.; Yang, J. K. W.; Simpson, R. E. Wide Bandgap Phase Change Material Tuned Visible Photonics. *Adv. Funct. Mater.* **2019**, *29* (6), 9.
(29) Wang, Q.; Lai, Y. Q.; Liu, F. Y.; Jiang, L. X.; Jia, M.; Wang, X. L. Sb_2S_3 nanorods/porous-carbon composite from natural stibnite ore as high-performance anode for lithium-ion batteries. *Trans. Nonferrous Met. Soc. China* **2021**, *31* (7), 2051−2061.
(30) Gutiérrez, Y.; Ovvyan, A. P.; Santos, G.; Juan, D.; Rosales, S. A.; Junquera, J.; García-Fernández, P.; Dicorato, S.; Giangregorio, M. M.; Dilonardo, E.; et al. Interlaboratory study on Sb_2S_3 interplay between structure, dielectric function, and amorphous-to-crystalline phase change for photonics. *iScience* **2024**, *27* (11), 111206.
(31) Wuttig, M.; Yamada, N. Phase-change materials for rewriteable data storage. *Nat. Mater.* **2007**, *6* (11), 824−832.
(32) Wang, J. M.; Wang, L.; Liu, J. Overview of Phase-Change Materials Based Photonic Devices. *IEEE Access* **2020**, *8*, 121211−121245.
(33) (33) Yang, R.; Lou, J.; Zhang, F.; Zhu, W.; Xu, J.; Cai, T.; Fu, Q.; Li, H.; Fan, Y. Active Control of Terahertz Toroidal Excitations in a Hybrid Metasurface with an Electrically Biased Silicon Layer. *Adv. Photonics Res.* **2021**, *2* (12), 2100103.
(34) Jiao, Y. A.; Lou, J.; Ma, Z. F.; Cong, L. Q.; Xu, X.; Zhang, B.; Li, D. C.; Yu, Y.; Sun, W.; Yan, Y.; Hu, S. D.; Liu, B. Y.; Huang, Y. D.; Sun, L.; Wang, R. D.; Singh, R.; Fan, Y. C.; Chang, C.; Du, X. H. Photoactive terahertz metasurfaces for ultrafast switchable sensing of colorectal cells. *Mater. Horz.* **2022**, *9* (12), 2984.
(35) Wang, Y. F.; Landreman, P.; Schoen, D.; Okabe, K.; Marshall, A.; Celano, U.; Wong, H. S. P.; Park, J.; Brongersma, M. L. Electrical tuning of phase-change antennas and metasurfaces. *Nat. Nanotechnol.* **2021**, *16* (6), 667−672.
(36) Abdollahramezani, S.; Hemmatyar, O.; Taghinejad, M.; Taghinejad, H.; Krasnok, A.; Eftekhar, A. A.; Teichrib, C.; Deshmukh, S.; El-Sayed, M. A.; Pop, E.; Wuttig, M.; Alu, A.; Cai, W.; Adibi, A. Electrically driven reprogrammable phase-change metasurface reaching 80% efficiency. *Nat. Commun.* **2022**, *13* (1), 11.
(37) Efthimiopoulos, I.; Buchan, C.; Wang, Y. J. Structural properties of Sb_2S_3 under pressure: evidence of an electronic topological transition. *Sci. Rep.* **2016**, *6*, 9.
(38) Avilez Garcia, R.G.; Meza Avendano, C.A.; Pal, M.; Paraguay Delgado, F.; Mathews, N.R. Antimony sulfide (Sb_2S_3) thin films by pulse electrodeposition: Effect of thermal treatment on structural, optical and electrical properties. *Mater. Sci. Semicond. Process* **2016**, *44*, 91−100.
(39) Delaney, M.; Zeimpekis, I.; Lawson, D.; Hewak, D. W.; Muskens, O. L. A New Family of Ultralow Loss Reversible Phase-Change Materials for Photonic Integrated Circuits: Sb_2S_3 and Sb_2Se_3. *Adv. Funct. Mater.* **2020**, *30* (36), 10.
(40) Essajai, R.; Hassanain, N. Molecular dynamics study of melting properties of gold nanorods. *J. Mol. Liq.* **2018**, *261*, 402−410.
(41) Shim, J. H.; Lee, B. J.; Cho, Y. W. Thermal stability of unsupported gold nanoparticle: a molecular dynamics study. *Surf. Sci.* **2002**, *512* (3), 262−268.
(42) Taylor, A. B.; Siddiquee, A. M.; Chon, J. W. M. Below Melting Point Photothermal Reshaping of Single Gold Nanorods Driven by Surface Diffusion. *ACS Nano* **2014**, *8* (12), 12071−12079.

https://doi.org/10.1021/acs.nanolett.5c00929
Nano Lett. 2025, 25, 7435−7441